Available online at www.sciencedirect.com
ScienceDirect
Trans. Nonferrous Met. Soc. China 24(2014) 626−631
Transactions of Nonferrous Metals Society of China
www.tnmsc.cn

Hot compression behavior and processing map of cast Mg−4Al−2Sn−Y−Nd alloy

Jing WANG[1], Bao-liang SHI[1], Yuan-sheng YANG[1,2]

1. Institute of Metal Research, Chinese Academy of Science, Shenyang 110016, China;
2. New Materials Research Institute of Shandong Academy of Sciences, Ji'nan 250014, China

Received 7 February 2013; accepted 8 May 2013

Abstract: The plastic flow behavior of a newly developed high ductility magnesium alloy, Mg−4Al−2Sn−Y−Nd, was investigated by hot compression from 200 to 400 °C with a strain rate of 1.5×10^{-3} to 7.5 s^{-1}. The results reveal that the strain rate sensitivity factor (m) of the alloy is much lower than that of the AZ31 alloy, which implies that the alloy should be more suitable for processing at high strain rate. The constitutive relationship of the alloy deformed at elevated temperature was obtained by plotting the experimental data. The stress exponent of the alloy is 10.33, which reveals that climb-controlled dislocations creep is the dominated deformation mechanism. The processing-map technique was used to determine the practical processing window. The proper deformation temperature and strain rate of the cast alloy were determined as 350−400 °C and 0.01−0.03 s^{-1}, respectively.
Key words: magnesium alloy; uniaxial compression; apparent activation energy; processing map

1 Introduction

There is increasing interests in the development of high performance wrought magnesium alloys because of the strong demands for mass reduction in aircraft, automotive and electronic industries [1−3]. However, the formability of magnesium alloys at ambient temperature is poor due to the limited slip systems with hexagonal lattice, which restricts their wide use [4]. At higher temperature (>250 °C), some non-basal slip systems of magnesium alloys are activated [5−7]. Therefore, it is safe to infer that the deformability of magnesium alloys will be increased at elevated temperature. Recently, a high ductility magnesium alloy, Mg−4Al−2Sn−Y−Nd, has been developed [8], which displays outstanding elongation of 23% at room temperature under as-cast condition. The new alloy provides great potentials to develop wrought magnesium alloys.

In order to obtain reasonable hot workability of the magnesium alloy, it is important to study the constitutive flow behavior of it and develop a processing map [9,10]. Based on the stress−strain relationships under various strain rates and temperatures, the constitutive equation can be developed to describe the mechanical response under various plastic deformation conditions. Three constitutive equations have been proposed to describe the deformation behavior of metals during hot working as follows [11]:

$$\dot{\varepsilon}\exp(Q/RT) = A_1\sigma^{n_1} \quad (1)$$

$$\dot{\varepsilon}\exp(Q/RT) = A_2\exp(\beta\sigma) \quad (2)$$

$$\dot{\varepsilon}\exp(Q/RT) = A[\sinh(\alpha\sigma)]^n \quad (3)$$

where $\dot{\varepsilon}$ is the strain rate; Q is the activation energy; R is the molar gas constant (R=8.314 J/K); T is the absolute temperature; and A, A_1, A_2, n_1, n, α, and β are the constants for given materials.

Equation (1) is known as Arrhenius relationship, and it is used in the case of low stress. Equations (2) and (3) are called hyperbolic sine relationship. The former is used in the case of high stress, and the latter is a unified semi-empirical relation.

The processing map is developed on the basis of dynamic materials model (DMM) [12]. The power dissipation efficiency could reflect the microstructural changes and identify the domain of dynamic

Foundation item: Project (2011BAE22B01-1) supported by the National Key Technology R&D Program; Project (2011DFA50903) supported by the International Science & Technology Cooperation Program of China
Corresponding author: Yuan-sheng YANG; Tel: +86-24-23971728; Fax: +86-24-23844528; E-mail: ysyang@imr.ac.cn
DOI: 10.1016/S1003-6326(14)63104-6

recrystallization. In addition, according to the flow instability criterion the instability regime in the processing map can be avoided. Therefore, the hot workability can be optimized by the processing map to secure the post-deformed properties.

The previous works indicated that hot deformation of common wrought magnesium alloys is a thermal activation course essentially and the constitutive behavior is in the form of hyperbolic sine relationship [13,14]. Recently, a new wrought magnesium alloy has been developed, but the constitutive behavior is lacking for this alloy. The aim of the present work is to understand the constitutive flow behavior of the Mg−4Al−2Sn−Y−Nd alloy and develop a processing map for hot working.

2 Experimental

The experimental material was the Mg−4Al−2Sn−Y−Nd magnesium alloy (abbreviated as ATWE4200) cast ingot. Cylindrical specimens (d8×12 mm) were cut from an as-cast ingot. The hot uniaxial compression tests were conducted on a Gleeble 3800 in argon atmosphere. The strain rate ($\dot{\varepsilon}$) and the deformation temperature (t) are in the range of 1.5×10^{-3}–7.5 s^{-1} and 200–400 °C, respectively, with a true strain of 0.6. In order to reduce the influence of friction, the Teflon tape was laid at the interface between the specimen and the crosshead. The specimens were heated up to the deformation temperature with a heating rate of 5 °C/s and held isothermally for 300 s prior to compression. Immediately after deformation, all the specimens were quenched in air to maintain their deformation microstructure.

3 Results and discussion

3.1 Flow stress behavior

Typical true stress−strain curves of the ATWE4200 alloy under various hot compression conditions are shown in Fig. 1. In the figure, three stages exist approximately in the curve. The flow stress initially increases sharply with increasing strain due to strain hardening, until it reaches a maximum stress value where dynamic softening occurs [15], and then it decreases continuously to a steady stress value owing to the dynamic balance between strain hardening and strain softening [16]. In general, the softening is attributed to the dynamic recovery (DRV) and the dynamic recrystallization (DRX) [17]. Besides, it should be noticed that the flow behavior is significantly influenced by the testing temperature and strain rate. At low temperature or high strain rate, apparent strain hardening occurs followed by softening. In contrast, at high temperature or low strain rate, a dynamic equilibrium between strain hardening and softening occurs at the very initial stage.

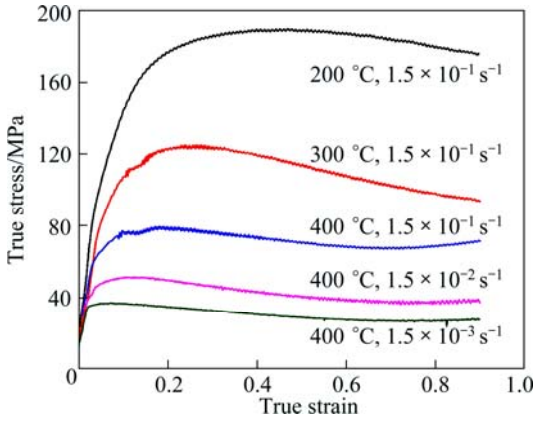

Fig. 1 True stress−true strain curves of ATWE4200 alloy hot compressed at different conditions

The peak stress is more relevant to practical application in industry. Figure 2 shows its relationship with deformation temperature and strain rate, respectively. It can be seen that at a given strain rate the peak stress decreases with increasing of the temperature. This is because at elevated temperature the critical resolved shear stress (CRSS) for slip systems, including basal slip, prismatic slip and pyramidal slip, decreases. And the cross-slip and dislocation climb operate more readily. The trend has been reported in the AZ31 alloy [18].

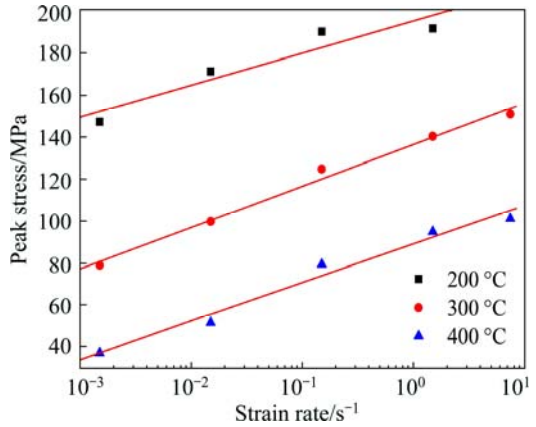

Fig. 2 Effect of strain rate on peak stress of ATWE4200 alloy at various temperatures

On the other hand, the peak stress increases with increasing the strain rate when the temperature is fixed, which is attributed to two reasons: 1) the increment of strain rate leads to higher density of dislocation at grain boundaries, thus, the stress is highly concentrated in specimen; 2) due to higher strain rate, there is no enough time for dynamic recrystallization, which is crucial to dynamic softening. Generally, the effect of strain rate on the mechanical properties can be described by the strain rate sensitivity factor (m) as follows:

$$m=\frac{\ln(\sigma_1/\sigma_2)}{\ln(\dot{\varepsilon}_1/\dot{\varepsilon}_2)} \tag{4}$$

According to Fig. 2 and Eq. (4), the m values of the ATWE4200 alloy are calculated to be 0.006, 0.101 and 0.154 at 200, 300 and 400 °C, respectively. Compared with the present alloy, the m values for AZ31 are much higher, 0.233 and 0.648 at 200 and 300 °C [19], respectively. It has been reported that the alloy with low m value is more suitable for high strain rate processing [9], thus the present alloy should be more suitable for processing at high strain rate.

3.2 Constitutive equation

3.2.1 Arrhenius relationship

The Arrhenius relation is described by $\dot{\varepsilon}\exp(Q/RT)$ as a power function of σ. The equations can be simplified to get the natural logarithms of both sides for Eq. (1) as follows:

$$\ln\dot{\varepsilon}=\ln A_1-Q/RT+n_1\ln\sigma \tag{5}$$

$$\frac{1}{n_1}=\left(\frac{\ln\sigma}{\ln\dot{\varepsilon}}\right)_T \tag{6}$$

In Fig. 3, the average value of n_1 can be determined to be 14.42 through the linear regression of $\ln\sigma$ versus $\ln\dot{\varepsilon}$. It has been reported that the value of stress exponent n_1 of Mg alloys could reflect the deformation mechanism at elevated temperature [20]. When n_1>5, climb-controlled dislocation creep is the predominate deformation mechanism [21].

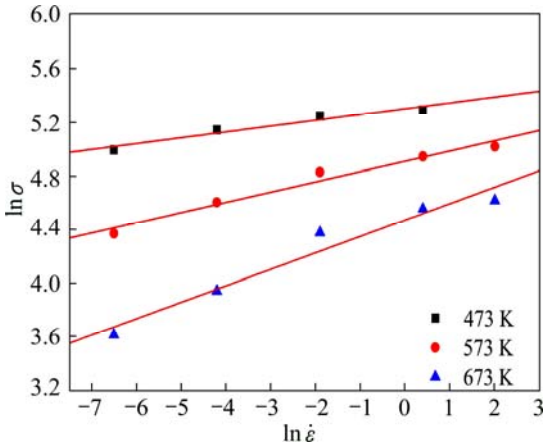

Fig. 3 Peak stress versus strain rate at different deforming temperatures based on power function model

According to Eqs. (5) and (6), the activation energy (Q) is calculated as follows:

$$Q_1=Rn_1\left[\frac{\partial\ln\sigma}{\partial(1/T)}\right]_{\dot{\varepsilon}} \tag{7}$$

where $\left[\frac{\partial\ln\sigma}{\partial(1/T)}\right]_{\dot{\varepsilon}}$ represents the slope of $\ln\sigma$ versus $1/T$. To calculate Q, $\ln\sigma$ is plotted versus $1000/T$ as shown in Fig. 4. The hot deformation activation energy derived from the experimental data is 195 kJ/mol which is higher than the value for AZ31 alloy, 112 kJ/mol, reported by GUO et al [22].

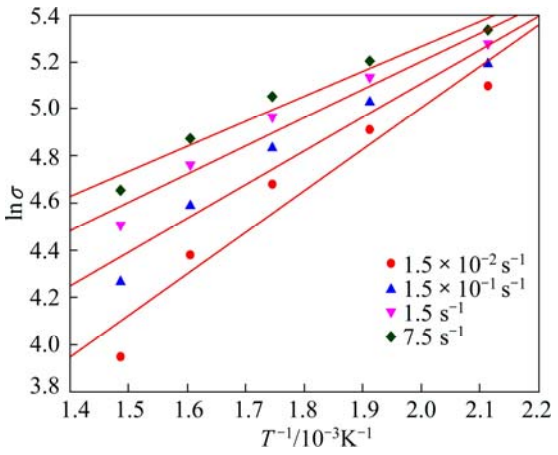

Fig. 4 Relationship between $\ln\sigma$ and $1/T$ at different strain rates

3.2.2 Hyperbolic relationship

The hyperbolic relation can be expressed by two kinds of equations. Equation (2) formulates $\dot{\varepsilon}\exp(Q/RT)$ as exponential function of σ, and equation (3) describes $\dot{\varepsilon}\exp(Q/RT)$ as hyperbolic function of σ. As abovementioned, the following equations can be derived from Eqs. (2) and (3), supposing $\alpha=\beta/n_1$.

$$\frac{1}{\beta}=\left(\frac{\sigma}{\ln\dot{\varepsilon}}\right)_T \tag{8}$$

$$Q_2=R\beta\left[\frac{\partial\sigma}{\partial(1/T)}\right]_{\dot{\varepsilon}} \tag{9}$$

$$\frac{1}{n}=\left(\frac{\ln[\sinh(\alpha\sigma)]}{\ln\dot{\varepsilon}}\right)_T \tag{10}$$

$$Q_3=Rn\left[\frac{\partial\ln\sinh(\alpha\sigma)}{\partial(1/T)}\right]_{\dot{\varepsilon}} \tag{11}$$

The stress exponent n, calculated with hyperbolic function, is about 10.33, similar with the value of n_1 determined by Arrhenius model. The result also manifests that the deformation is controlled by dislocation climbing. The values of the activation energy calculated through Eqs. (9) and (11) are 188 and 191 kJ/mol, respectively, which is in agreement with the approach of Eq. (7). In addition, it should be noted that the activation energy calculated with both Arrhenius relation and hyperbolic relations is higher than the activation energy for pipe diffusion (92 kJ/mol) and activation energy for lattice self-diffusion (135 kJ/mol) [23]. Similar phenomenon has been reported in some Mg

alloys containing rare earth [24].

Essentially, the activation energy is related to movability of the dislocations. The secondary phase particles could hinder dislocation movement, which leads to higher energy for cross slip and dislocation climbing, and in consequence activation energy is increased. Figure 5 shows the interaction between dislocation and particle in the alloy deformed at 400 °C with a strain rate of 0.15 s^{-1}. It can be seen that the Al_2RE particle can effectively hinder dislocation movement, which results in dislocation tangle in the front of the particle. Therefore, it is safe to relate the high activation energy of the present alloy to existence of the high stable Al_2RE phase.

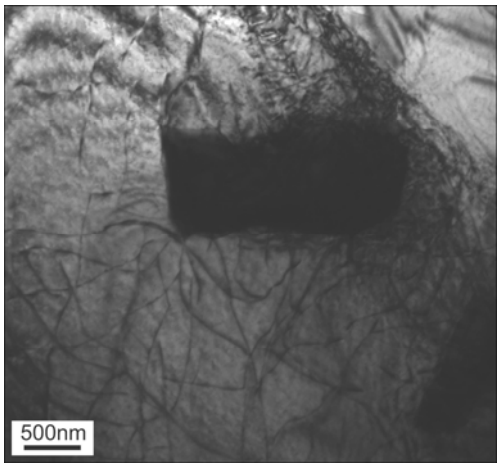

Fig. 5 TEM bright-field image of alloy deformed at 400 °C with strain rate of 0.15 s^{-1}

3.2.3 Model validation

In general, Eqs. (1)−(3) can be expressed in the forms as follows:

$$\ln Z = n_1 \ln\sigma + \ln A_1 \tag{12}$$

$$\ln Z = \beta\sigma + \ln A_2 \tag{13}$$

$$\ln Z = n \ln[\sinh(\alpha\sigma)] + \ln A \tag{14}$$

where Z is the Zener-Hollomon parameter that is usually expressed in terms of temperature compensated strain rate as follows:

$$Z = \dot{\varepsilon}\exp(Q/RT) \tag{15}$$

Figure 6 shows the linearly fitted lines of $\ln Z$ versus $\ln\sigma$, $\ln Z$ versus σ, and $\ln Z$ versus $\ln[\sinh(\alpha\sigma)]$ at different deformation temperatures, respectively. The pre-exponential constants A_1, A_2, and A can be obtained by calculating the y-intercept of the lines. However, it should be noticed that the constant values corresponding to Eqs. (12) and (14) change dramatically with deformation temperature. Compared with power function and hyperbolic function, pre-exponential constant with exponential function changes very little, as shown in Fig. 6(b). The result reflects that the actual peak stress is

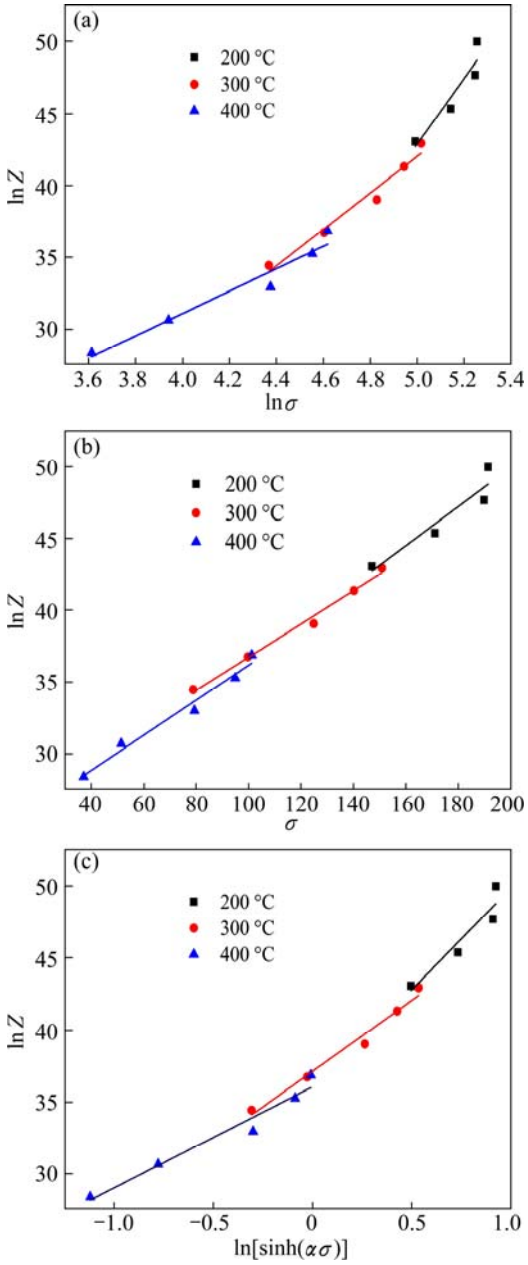

Fig. 6 Linearization data of $\ln Z$—$\ln\sigma$ (a), $\ln Z$—σ (b), and $\ln Z$—$\ln[\sinh(\alpha\sigma)]$ (c) at different deformation temperatures

very close to the theoretical peak stress calculated by Eq. (13). Therefore, Eq. (2) is more suitable to describe the deformation behavior of ATWE4200 alloy. When Q_2 is substituted into Eq. (2), A_2 can be figured out. Thus, the plastic flow constitutive semi-empirical model for $\dot{\varepsilon}$, σ and T can be expressed as

$$\dot{\varepsilon} = 1.98\times10^9 \exp(0.1218\sigma_p)\exp\left(-\frac{181000}{RT}\right) \tag{16}$$

3.3 Processing map

The processing-map technique has been used in hot working of Mg alloys to understand their constitutive

flow behavior and optimize the hot workability. Based on DMM, the workpiece is considered a dissipater of power, and the characteristics of power dissipation through microstructural changes are described in terms of an efficiency of power dissipation which is defined by

$$\eta = \frac{2m}{m+1} \tag{17}$$

where m is the strain rate sensitivity of flow stress given by $(\partial \ln \dot{\varepsilon})/(\partial \ln \sigma)$. The variation of efficiency with deformation temperature and strain rate constitutes a processing map. Each domain corresponds to a specific microstructural characteristic. High efficiency of power dissipation indicates dynamic recrystallization or local flow instability, which can be identified by investigating the microstructure of the specimen.

Furthermore, based on the irreversible thermodynamics the continuum instability criterion of large plastic flow can be defined by a dimensionless factor $\xi(\dot{\varepsilon})$ as follows:

$$\xi(\dot{\varepsilon}) = \frac{\partial \ln[m/(m+1)]}{\partial \ln \dot{\varepsilon}} + m \le 0 \tag{18}$$

The variation of $\xi(\dot{\varepsilon})$ constitutes the instability map that is superimposed on the processing map to delineate the instability regimes for the negative $\xi(\dot{\varepsilon})$ values.

Figure 7 exhibits the processing map at the true strain of 0.3 by superimposing the power-dissipation map on the flow instability map. The bigger values of η appear at the middle right corner of the map corresponding to higher deformation temperatures and medium strain rates, while the smaller values can be seen at both the upper left corner corresponding to lower deformation temperatures and the upper right corner corresponding to higher deformation temperatures with high strain rates. In addition, the map exhibits three instability domains (shadow areas) in the temperature and strain rate ranges: (I) t=200−270 °C and $\dot{\varepsilon}$=0.003−0.3 s^{-1}; (II) t=270−330 °C and $\dot{\varepsilon}$=0.4−1.5 s^{-1}; (III) t=350−400 °C and $\dot{\varepsilon}$=0.06−0.15 s^{-1}. However, compared with the conventional AZ31 alloy, the hot deformation processing window for the alloy is relatively large [25]. High efficiency domain, where instability area can be avoided, corresponds to appropriate processing area, which could yield out sufficiently recrystallized microstructure. Taking into account the production efficiency and preventing high temperature oxidation by local overheat, the practical processing window can be determined as t=350−400 °C and $\dot{\varepsilon}$=0.01−0.03 s^{-1}. It seems that the proper strain rate for Mg−4Al−2Sn−Y−Nd alloy is apparently higher than that of AZ80 and AZ31 alloys [25,26], which further indicates that the alloy is suitable for hot processing at high strain rate.

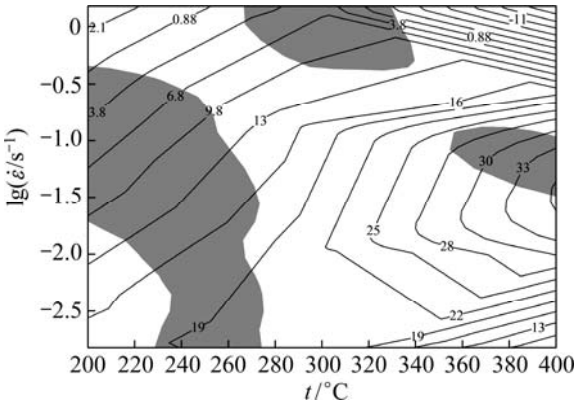

Fig. 7 Processing map at true strain of 0.3 by superimposing power−dissipation map on flow instability map (Light dark area stands for value of $\xi(\dot{\varepsilon}) < 0$)

4 Conclusions

1) Due to possessing relatively low strain rate sensitivity, Mg−4Al−2Sn−Y−Nd alloy could be more suitable for hot processing at high strain rate.

2) Apparent activation energy of the alloy is 188 kJ/mol, and the stress exponent is 10.33. The exponent function is more suitable to describe the plastic flow behavior of the studied magnesium alloys.

3) The processing-map result shows that the rational processing window of the cast alloy should be 350−400 °C and $\dot{\varepsilon}$=0.01−0.03 s^{-1}.

References

[1] MORDIKE B L, EBERT T. Magnesium properties—Applications—potential [J]. Materials Science and Engineering A, 2001, 302: 37−45.

[2] KULEKCI M K. Magnesium and its alloys applications in automotive industry [J]. International Journal of Advanced Manufacture Technology, 2008, 39: 851−865.

[3] FRIEDRICH H, SCHUMANM S. Research for a “new age of magnesium” in the automotive industry [J]. Journal of Material Processing Technology, 2001, 117: 276−281.

[4] WU D, CHEN R S, HAN E H. Excellent room-temperature ductility and formability of rolled Mg−Gd−Zn alloy sheets [J]. Journal of Alloys and Compounds, 2011, 509: 2856−2863.

[5] LI L, ZHANG X, DENG Y, TANG C. Superplasticity and microstructure in Mg−Gd−Y−Zr rolled sheet [J]. Journal of Alloys and Compounds, 2009, 485: 295−299.

[6] YANG X, MIURA H, SAKAI T. Dynamic evolution of new grains in magnesium alloy [J]. Materials Transitions, 2003, 44: 197−203.

[7] TAN J C, TAN M J. Dynamic continuous recrystallization characteristics in two stage deformation of Mg−3Al−1Zn alloy sheet Mater [J]. Materials Science and Engineering A, 2003, 339: 124−132.

[8] WANG J, FU J W, DONG X G, YANG Y S. Microstructure and mechanical properties of as-cast Mg−Al−Sn−Y−Nd alloy [J]. Material & Design, 2012, 36: 432−437.

[9] ZHENG X W, LUO A A, DONG J, SACHDEV A K, DING W J. Plastic flow behavior of a high-strength magnesium alloy NZ30K [J].

Materials Science and Engineering A, 2012, 532: 616−622.
[10] YU H, YU H S, KIM Y M, YOU B S, MIN G H. Hot deformation behavior and processing maps of Mg−Zn−Cu−Zr magnesium alloy [J]. Transactions of Nonferrous Metals Society of China, 2013, 23: 756−764.
[11] MAKSOUD I A, AHMED H, RODEL J. Investigation of the effect of strain rate and temperature on the deformability and microstructure evolution of AZ31 magnesium alloy [J]. Materials Science and Engineering A, 2009, 504: 40−48.
[12] SHESHACHARULU T, PRASAD Y V R K. Modeling of hot deformation for microstructural control [J]. International Materials Reviews, 1998, 43: 243−258.
[13] WU H Y, YANG J C, LIAO J H, ZHU F J. Dynamic behavior of extruded AZ61 Mg alloy during hot compression [J]. Materials Science and Engineering A, 2012, 535: 68−75.
[14] LI L, ZHANG X M. Hot compression deformation behavior and processing parameters of a cast Mg−Gd−Y−Zr alloy [J]. Materials Science and Engineering A, 2011, 528: 1396−1401.
[15] SAKAI T, JONAS J J. Dynamic recrystallization: Mechanical and microstructural considerations [J]. Acta Metallurgica, 1984, 32: 189−209.
[16] BARNETT M R. Influence of deformation conditions and texture on the high temperature flow stress of magnesium AZ31 [J]. Journal of Light Metals, 2001, 1: 167−177.
[17] YU K, LI W X, ZHAO J, MA Z Q, WANG R C. Plastic deformation behaviors of a Mg−Ce−Zn−Zr alloy [J]. Scripta Materialia, 2003, 48: 1319−1323.
[18] FU P H, PENG L M, JIANG H Y, CHANG J W, ZHAI C Q. Effects of heat treatments on the microstructures and mechanical properties of Mg−3Nd−0.2Zn−0.4Zr (wt.%) alloy [J]. Materials Science and Engineering A, 2008, 486: 183−192.
[19] TAN C W, XU S N, WANG L, CHEN Z Y, WANG F C, CAI H N. Effect of temperature on mechanical behavior of AZ31 magnesium alloy [J]. Transiations of Nonferrous Metals Society of China, 2007, 17: 41−45.
[20] TAKARA A, NISHIKAWA Y, WATANABE H, SOMEKAWA H, HIGASHI M K. Secondary processing of AZ31 magnesium alloy concomitant with grain growth or dynamic recrystallization [J]. Materials Transitions JIM, 2004, 45: 2377−2382.
[21] HIRAI K, SOMEKAWA H, TAKIGAWA Y, HIGASHI K. Effects of Ca and Sr addition on mechanical properties of a cast AZ91 magnesium alloy at room and elevated temperature [J]. Materials Science and Engineering A, 2005, 403: 276−280.
[22] GUO Q, YAN H G, ZHANG H, CHENAND Z H, WANG Z F. Behaviour of AZ31 magnesium alloy during compression at elevated temperatures [J]. Materials Science and Technology, 2005, 21: 1349−1354.
[23] SOMEKAWA H, HIRAI K, WATANABE H, TAKIGAWA Y, HIGASHI K. Dislocation creep behavior in Mg−Al−Zn alloys [J]. Materials Science and Engineering A, 2005, 407: 53−61.
[24] WU W X, JIN L, DONG J, DING W J. Prediction of flow stress of Mg−Nd−Zn−Zr alloy during hot compression [J]. Transactions of Nonferrous Metals Society of China, 2012, 22: 1169−1175.
[25] XIAO M, ZHOU Z, HUANG G J, WANG B S. Hot deformation behavior and processing maps of AZ31 magnesium alloy [J]. Materials for Mechanical Engineering, 2010, 34: 18−21.
[26] HUANG S H, ZHAO Z D, XIA Z X, CAI H Y, KANG F, HU C K, SHU D Y. Study on high-temperature deformation behavior and processing map of AZ80 alloy [J]. Rare Metal Materials and Engineering, 2010, 39: 848−852. (in Chinese)

铸造 Mg−4Al−2Sn−Y−Nd 镁合金的热压缩行为与加工图

王 晶[1]，史宝良[1]，杨院生[1,2]

1. 中国科学院 金属研究所，沈阳 110016；
2. 山东省科学院 新材料研究所，济南 250014

摘 要：利用热压缩实验研究一种新型的具有优异室温塑性的 Mg−4Al−2Sn−Y−Nd 镁合金的高温流变行为，变形温度为 200~400 °C，应变速率为 1.5×10^{-3}~7.5 s^{-1}。结果表明：合金的应变速率敏感因子(m)在不同变形温度下均明显小于 AZ31 镁合金的 m 值，因此该合金适合在高应变速率下进行热加工。在真应力−应变曲线基础上，建立 Mg−4Al−2Sn−Y−Nd 镁合金高温变形的本构方程，并计算得到合金的应力指数为 10.33，表明合金在高温下主要的变形机制为位错攀移机制。同时，利用加工图技术确定合金的最佳高温变形加工窗口，即变形温度在 350~400 °C 之间，应变速率在 0.01~0.03 s^{-1}。

关键词：镁合金；单轴压缩；激活能；加工图

(Edited by Chao WANG)